Aggregation of Lipid A Variants: a Hybrid Particle-Field Model

Antonio De Nicola,[1,*] Thereza A. Soares,[2] Denys E. S. Santos,[2] Sigbjørn Løland Bore,[3] G. J. Agur Sevink,[4] Michele Cascella,[3] Giuseppe Milano[1]

[1]*Department of Organic Material Science, Yamagata University, Yonezawa 992-8510, Japan.*

[2]*Department of Fundamental Chemistry, Universidade Federal de Pernambuco, Cidade Universitária, Recife, PE 50740-560, Brazil*

[3]*Department of Chemistry and Hylleraas Centre for Quantum Molecular Sciences, University of Oslo, P.O. Box 1033, Blindern, 0315 Oslo, Norway*

[4]*Leiden Institute of Chemistry, Leiden University, P. O. Box 9502, 2300 RA Leiden, The Netherlands.*

Abstract

Lipid A is one the three components of bacterial lipopolysaccharides (constituting the outer membrane of Gram-negative bacteria) and is recognized to have an important biological role in the inflammatory response of the immune system. Its biological activity is modulated by the number of acyl-chains that are present in the lipid and by the dielectric medium, i.e, the type of counter-ions, through electrostatic interactions. In this paper, we report a coarse-grained model of poly-acyl Lipid A based on the hybrid particle field molecular dynamics approach (hPF-MD). In particular, we investigate the stability of Lipid A bilayers for two different acyl-chains, hexa and tetra. Comparing particle density profiles along bilayer cross-sections, we find good agreement between our hPF-MD and reference all-atom simulation results for both bilayers.. Moreover, we validate our model by simulating the self-assembly of a lamellar phase from an initially random distribution of Lipid Amolecules with N^{2+} counterions in water. Finally, we test the stability of a vesicle that is composed of hexa-acylated Lipid A in water. Bothbilayer aggregates and a spherical vesicle are found

to be stable upon simulation with the proposed model, and also the phase behavior of Lipid A/Ca^{2+}/water mixture is correctly reproduced.

1. Background

Lipopolysaccharides (LPS) are the major lipid constituents of the external leaflet of an asymmetric outer membrane (OM) in Gram-negative bacteria.[1,2] The OM acts as a structural and functional barrier against penetration of xenobiotic agents like hydrophobic antibiotics, digestive enzymes, heavy metals, detergents, or bile salts.[3] The LPS molecule can contain three different regions: (i) the polymeric *O*-antigen (repetitive monosaccharide subunits) responsible for the bacterium immunospecificity,[4] (ii) a branched oligosaccharide brush (composed of 8-12 monosaccharide units) and (iii) a Lipid A unit (composed of typically 4-6 acyl chains attached to a phosphorylated glucosamine disaccharide) responsible for the anchoring of the LPS leaflet onto the phospholipid leaflet of the OM.[5,6] Lipid A has a fundamental biological role as a stimulator of the inflammatory response by the immune system.[7–9] The immune response due to the presence of Lipid A is modulated by variations of its particular chemical structure, such as the number, length and position of acyl chains, as well as the overall molecular charge.[9–11]

The phase diagram of Lipid A in water includes four three-dimensional aggregation states: lamellar (L), hexagonal (H_I,) inverted hexagonal (H_{II}) and non-lamellar cubic (Q).[9,12] The relative stability of these aggregation states depends on environmental conditions (pH, temperature, ionic strength, cation types) as well as on the chemical structure of Lipid A. It is understood that these external and internal parameters particularly affect the Lipid A cross-sectional area of the hydrophobic part (the hydrocarbon chains), which gives rise to
 sa specific aggregation state.[9–11]

In the past decades, several MD studies have considered LPS and Lipid A. In particular, several all-atom[7,13–19] and coarse-grained (CG) models[5,20–23] have been applied and are continuously improved.[14,15,18] Despite this progress, simulating large systems and/or phenomena occurring on

time scales larger than the μs remains a hugre challenge, even for CG models. Overcoming the limitations may be achieved by developing models for lipopolysaccharides within a density-functional concept,[24] and in particular by adopting the hybrid particle-field/molecular dynamics (hPF-MD) approach.[25–27] The main advantage of hPF-MD is that non-bonded pair interactions between particles are replaced by the evaluation of an external potential based on the local particle density, which, in combination with an efficient parallelization scheme,[28] makes it possible to overcome the current time and scale limits of standard MD force fields (FFs) while retaining a sufficiently high molecular resolution to retain chemically resolved moieties. Past studies have demonstrated the ability of this approach to simulate structure formation in diverse soft matter systems, including lamellar and non-lamellar phospholipid moieties,[29–31] biocompatible block-copolymers,[32,33] non-charged surfactants,[34,35] and peptides.[36]

Recently, Zhu *et al.* introduced an efficient scheme based on the Ewald Summation to treat electrostatic interactions within the hPF-MD framework.[37] In particular, charged particles interact with an external electrostatic potential that is derived from the charge density, in equivalence to the mean-fieldpotential that is used to evaluate non-bonded interactions. Some of us reported a systematic study of the relative dielectric constant, which was matched to reproduce structural properties of SDS surfactant aggregates in water and to check the stability of POPG bilayer in water.[38] This study showed that, by an appropriate choice of the relative dielectric constant, it is possible to reproduce the self-assembly characteristics and stability of the aggregates (micellar or bilayer). An extension of the electrostatic treatment in the hPF-MD approach was introduced by Bore *et al,* by introducing a spatially resolved dielectric which depends on the local density fields of the different species.[39]

In this paper, we report on the development of specific hybrid CG model for the biologically relevant Lipid A (hexa- and tetra-acyl chains). We show that the hPF-MD model does not only reproduce the structural properties of atomistic simulations of hexa- and tetra-acylated Lipid A bilayers, but also constitutesa Lipid A phase diagram and vesicle aggregate structure that is highly consistent with experimental measurements *in vitro*.

2. Methods

2.1 The hPF-MD approach

In hPF-MD the total energy of the system is written as:

$$H = \sum_{m=1}^{N_{mol}} H_0(\{r\}_m) + W[\{\phi(r)\}] + W_{el}[\rho(r)], \quad 1$$

where $H_0(\{r\}_m)$ is the Hamiltonian of a single, non-interacting molecule m, $W[\{\phi(r)\}]$ is an interaction energy functional that depends on the particle density $\{\phi(r)\}$, and $W_{el}[\rho]$ is the total electrostatic energy, dependent on the charge density ρ. We employ the functional form for $W[\phi(r)]$:

$$W[\{\phi(r)\}] = \frac{1}{2\phi_0} \int dr k_B T \sum_{K'} \chi_{KK'} \phi_K(r)\phi_{K'}(r) + \frac{1}{\kappa}(\sum_K \phi_K(r) - \phi_0)^2, \quad (2)$$

as originally introduced.[25] Here k_B is the Boltzmann constant, T is the temperature of the system and $\phi_K(r)$ represents the coarse-grained number density of species K at position $\boldsymbol{r}$ and ϕ_0 is the total number density of the system. $\chi_{KK'}$ is the mixing energy term between species K, K', and κ is a compressibility term regulating the local fluctuations of the density. Under this assumption, particles of a generic type K are subject to an external potential of the form [25]:

$$V_K(r) = \frac{\delta W}{\delta \phi(r)} = \frac{1}{\phi_0} \quad (3)$$

The electrostatic energy of the system $W_{el}[\rho]$ is defined as:

$$W_{el}[\rho] = \frac{1}{2} \int dr \, \rho(r)\psi(r), \quad (4)$$

where the electrostatic potential ψ is governed by the Poisson equation:

$$-\nabla^2 \psi(r) = \frac{\rho(r)}{\epsilon_r \epsilon_0} \qquad (5)$$

ϵ_r is the relative dielectric constant of the medium and ϵ_0 is the vacuum permittivity. The computation of $\psi(r)$ is performed using the recently developed adapted PME-approach as in references [37,38].

The calculation of the molecular forces is done by a particle-mesh approach where $\phi_K(r)s$ are computed on a grid, and their spatial derivatives estimated by finite difference. In the present work, the density gradients are calculated by a rotational invariant finite-difference stencil developed by Alfaraj *et al.*[40], as implemented for hPF-MD by Sevink *et al* [41]. A complete description of the hPF-MD method and its extension to electrostatics interactions can be found in refs.[25,37–39,42].

2.2 hPF-MD CG Model of Lipid A.

In this study, the single-molecule Hamiltonian $H_0(\{r\}_m)$ is based on a CG representation of both Lipid A, the ions, and the solvent (**Figure 1**). All intramolecular interactions have the same functional form as in standard force fields, [25] using the parameters developed in our previous studies,[29,37] apart from the length l_B between two L bead types. Specifically, we employ lengths $l_B = 0.47$ nm for hexa- and $l_B = 0.34$ nm for the tetra-acylated Lipid A in order to improve their agreement with the all atom structures. A complete list of bonded FF parameters for Lipid A is reported in the Supporting Information.
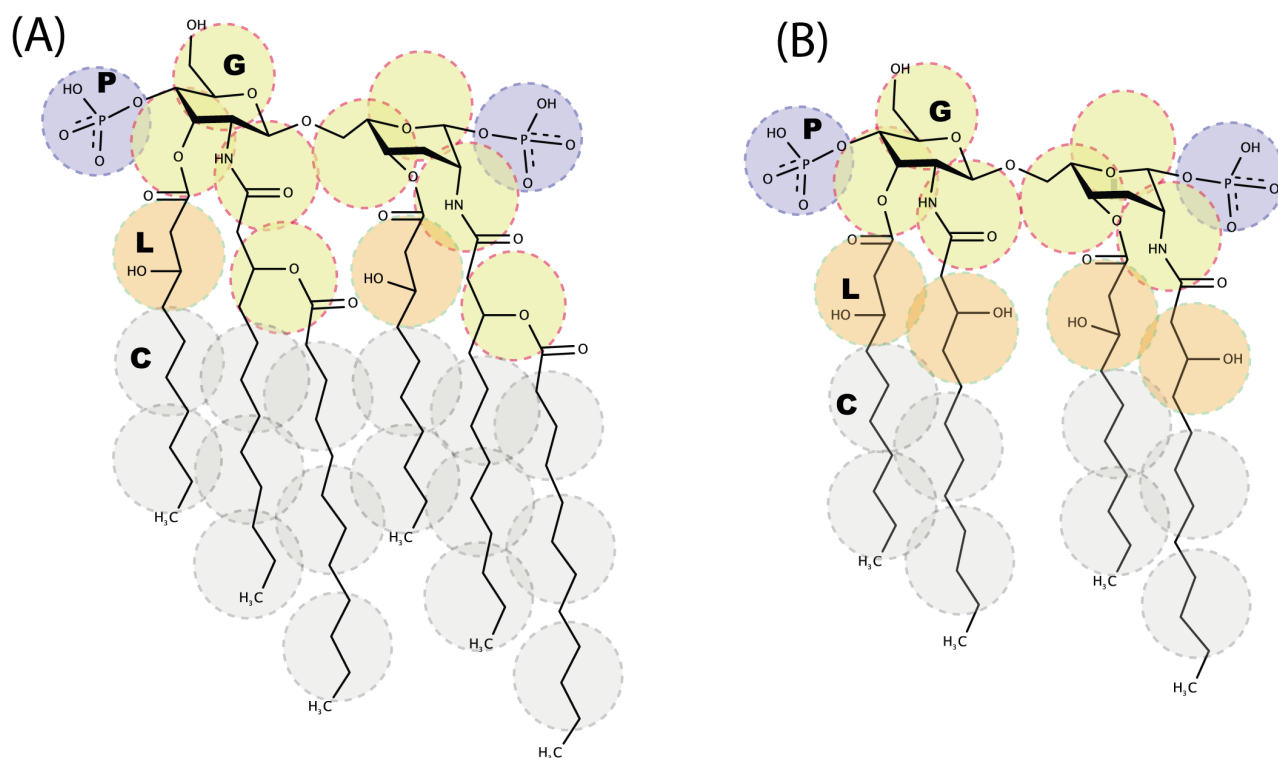
Figure 1. Chemical structures of (A) hexa- and (B) tetra-acylated forms of Lipid A, and a schematic overlay of the corresponding coarse-grained representation used in this work. Different bead types are indicated by the letters P, G, L, C and the color scheme. The counter-ion bead (N), and the water bead (W), representing four H_2O molecules, are not shown in the figure.

The mean-field Flory-Huggins $\chi_{KK'}$ parameters were first estimatedfrom the Martini force field Lennard-Jones binding energies,[43] and then further optimized to provide the best correspondence to the all-atom reference data. The final $\chi_{KK'}$ parameters used in all simulations are reported in **Table 1.**.

Table 1. Interaction matrix $\chi_{KK'} \times RT (kJmol^{-1})$ for the Lipid A/counter-ion/water system.

$\chi_{KK'} \times RT$	L	P	G	C	N (Counter-ion)	W (Water)
L	0	0	4.5	13.25	0	0
P	0	0	4.5	20	-7.2	-3.6
G	4.5	4.5	0	8.3	0	4.5
C	13.25	20	8.3	0	13.25	33.75
N (Counter-ion)	0	-7.2	0	13.25	0	0

W (Water)	0	-3.6	4.5	33.75	0	0

2.3 hPF-MD simulations of Lipid-A Membranes.

The hPF-MD simulations forboth the hexa- and tetra-acylated Lipid A bilayers start from membranes built using the all-atom results that were published in [19] (See **Scheme S1** in the Supporting Information). In particular, the area per lipid A_L for hexa- (1.53 nm^2) and tetra-acylated (1.2 nm^2) membrane systems is in agreement with experimental values.[44,45] Systems were neutralized by the addition of divalent cation beads randomly placed within a distance of 0.5 nm from the P beads in the Lipid A bilayer, and solvated by adding water beads using the Packmol package.[46] For the self-assembly simulations, the lipids were randomly distributed in the simulation box, whereas for the vesicle simulation,Packmol was used to build the initial state of the system.[46] The composition of all simulated systems can be found in **Table 2**.

hPF-MD simulations were performed with the OCCAM MD software.[42] A time step of 0.03 ps and a mesh size of $l = 0.57$ nm were used for all simulations. All simulations consider a NVT ensemble, with a temperature $T = 300$ K that is kept constant by the Andersen thermostat[47] with a collision frequency of 5 ps^{-1}. kept. The density field was updated every 100 time steps. Both the density update time and the mesh size were chosen to give good reproduction of the reference atomistic simulations, as reported in our previous works.[29,31–34]

2.4 Simulations of All-Atom Lipid A Membranes.

Benchmark all-atom MD simulations were performed for both the hexa- and tetra-acylated forms of Lipid A as previously described,[20] using an extension of the GROMOS 53A6 force field[20,48] in conjunction with the SPC water model.[49] MD simulations were performed in the NPT ensemble with a time step of 2.0 fs at 300 K and 1 bar. Bond lengths within the solute and the geometry of water molecules were constrained using the LINCS algorithm.[50] The temperatures of solute and solvent were controlled by separately coupling them to a velocity rescaling thermostat with a

relaxation time of 0.4 ps.[44] The pressure was maintained via the Berendsen pressure coupling algorithm with a semi-isotropic coordinate scaling coupling, using a coupling constant of 1 ps and an isothermal compressibility of 4.5×10^{-5} bar^{-1}.[45] Long-range electrostatic correction was applied using the Particle-Mesh Ewald (PME) approximation beyond a cut-off of 1.2 nm, with a fourth order interpolation of charges and a 0.16 nm Fourier spacing. Nonbonded pair lists were updated every 5 steps using a single cut-off scheme for atom pairs beyond a cut-off of 1.2 nm. The systems were first equilibrated for 100 ns to converge the area per lipid molecule, followed by an additional 400 ns simulation for data production. All-atom simulations were performed using the GROMACS 4.5.4 software suite.[51]

Table 2. Composition of the system simulated in this work.

System	Method	Lipid A molecules (Hexa-acyl)	Lipid A molecules (Tetra-acyl)	Counter ions	W beads	Box size *(x,y,z)* [nm^3]	Time [ns]
HPF1	hPF-MD	256	-	256 N^{2+}	9556	14.45 x 13.34 x 9.19	300
HPF2	hPF-MD	256	-	512 N^{+}	9483	14.08 x 12.99 x 9.35	300
HPF3	hPF-MD	-	128	256 N^{2+}	4125	13.62 x 5.33 x 7.86	300
HPF4	hPF-MD	1200	-	1200 N^{2+}	70000	22.0 x 22.0 x 22.0	4200
HPF5	hPF-MD	1400	-	1400 N^{2+}	15000	17.0 x 17.0 x 17.0	3550
HPF6	hPF-MD	644	-	644 N^{2+}	221235	30.0 x 30.0 x 30.0	1200
AA1	All-atom	128	-	128 Ca_2^{+}	4518	13.47 x 7.30 x 9.02	400
AA2	All-atom	128	-	256 Na^{+}	4474	13.71 x 5.36 x 8.00	400

3. Results

Effect of the dielectric constant ε_r on the stability of Lipid A bilayer. Appropriate calibration of the effective dielectric constant ϵ_r is fundamental for the correct description of charged lipid bilayers, as demonstrated by past work on a POPG membrane.[38] For this reason, we first investigated the stability of Lipid A bilayers for a range of values of the relative dielectric constant.

Starting from an initial CG configuration of hexa-acylated Lipid A that is mapped from the reference atomistic configuration (HPF1, **Table 2**), we ran four hPF-MD simulations, each 300 ns long, for four values of the relative dieclectric permittivity $\epsilon_r = 1,5,15,80$. The corresponding average structures and density profiles for the different chemical moieties along the direction normal to the plane of the bilayer are shown in **Figure 2**.
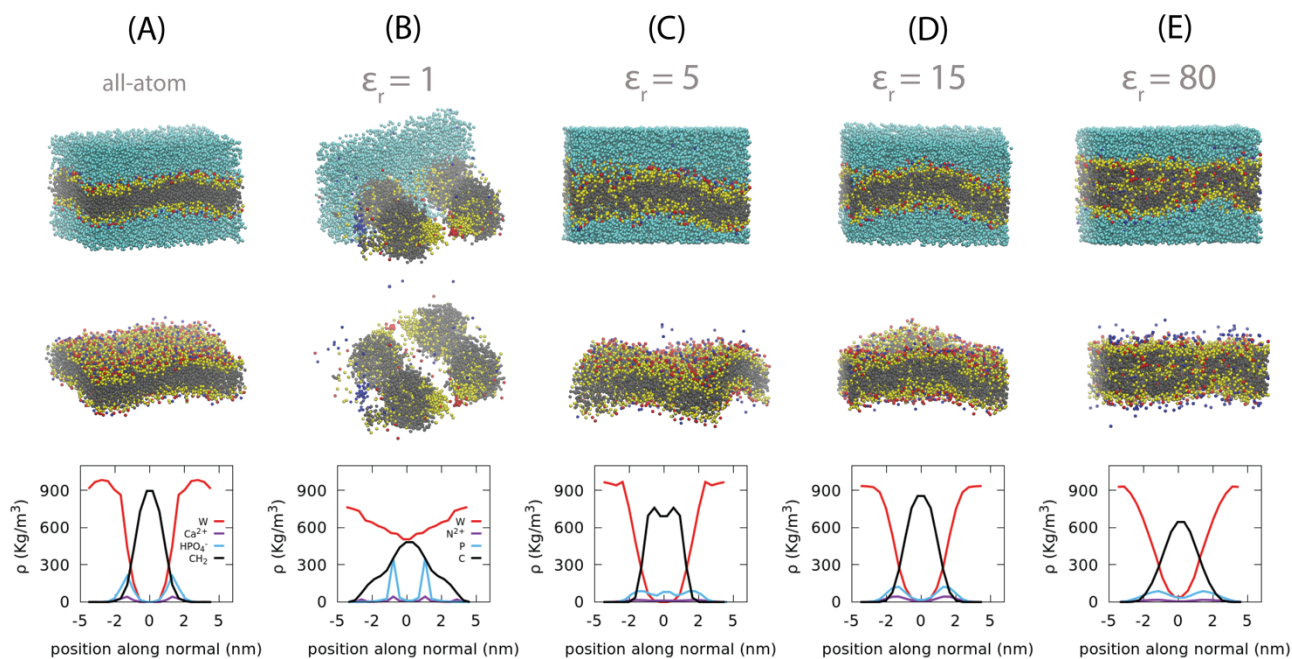

Figure 2. **Equilibrated structures of Lipid A bilayers.** *Top panels:* Representative snapshots of equilibrium configurations for (A) all-atom and (B-E) hPF-MD simulations of hexa-acylated Lipid A for different values of the relative dielectric constant (ϵ_r). The color scheme for CG bead types is: P (red), G and L (yellow), C (gray), N^{2+} (blue), and W (cyan). The same configuration is also shown without water beads for the sake of clarity. *Bottom panels:* Average mass density profiles corresponding to the systems shown above.

As expected, the organization of lipid A within the bilayers depends on the value of the dielectric constant (**Figure 2**). For the lowest value ($\epsilon_r = 1$), we obtain an unstable bilayer with a structure that is completely disrupted within the first 30 ns of simulation, while the global lamellar structure of the membrane is maintained for larger values of ϵ_r. hPF-MD simulations for $\epsilon_r = 15$ (**Figure 2D**) yield a stable bilayer structure within the time scale of simulation, and the density profiles of the atomistic reference system are most accurately reproduced. For $\epsilon_r = 5$ and 80, the density profiles indicate that the organization of Lipid A inside the membrane does not match: in both cases, we observe strong

surface undulation and a migration of the hydrophilic sites to the midplane of the bilayer (see snapshots with $\epsilon_r = 80$), with negatively charged P beads being distributed along the whole cross-section of the membrane (**Figures 2C,E**), indicating that lipids are tilted by an angle that is greater than 45 degrees (**Figure 2E**).

A closer comparison of the calculated density profiles for the all-atom reference (AA1, **Table 2**) and the hPF-MD simulations at $\epsilon_r = 15$, further substantiates the semi-qualitative agreement between the two models (**Figure 3**). In particular, data for the two types of simulation agree well in terms of the symmetric distribution of the peaks, the bilayer thickness D_{HH} as measured from the distance between P-P sites (3.82 nm for the reference system and 3.74 nm in hPF-MD), and in terms of the location of the phosphate groups in the bilayer and the distribution of the acyl tails. The hPF-MD density profiles have a slightly broader signature than of the all-atom reference,consistent with what has been previously reported for other lipid bilayers. This finding can be attributed to the softness of the potential employed in the hPF model. The largest discrepancy between hPF-MD and the all-atom models is the broader distribution of N^{2+} counterions in the hPF-MD model, when compared to the all-atom Ca^{2+} profile, and their penetration into the lipophilic region of the bilayer (**Figure 4**). Similar findings for the ions were previously reported for the DOPG membrane.[38] They can be attributed to both the soft nature of the hPF-MD potentials and the lack of an explicit change in the dielectric environment between the solvent and lipid phases.
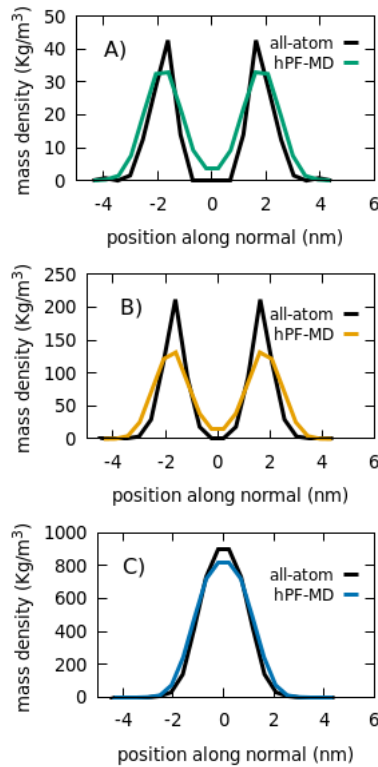
Figure 3. Comparison of density profiles for the hexa-acylated Lipid-A HPF-MD simulation for $\epsilon_r = 15$ and the reference atomistic simulation: (A) Ca^{2+}/N, (B)HPO_4^-/P, and (C) CH_2/C moieties.

Effect of the counterion valence on the bilayer structure. It was previously shown that divalent cations induce considerable changes in the physico-chemical parameters of LPS membranes, such as hydration, acyl chain mobility, and aggregation state, when compared to monovalent cations.[7,52,53] Divalent cations increase the liquid-crystal transition temperature (T_c) values and acyl chain order, whereas Na^+ increases the hydration of the LPS leaflet.[3,7,54–56] Therefore, we investigated how well the hPF-MD model reproduces the different effects that divalent and mono-valent counterions have on the stability and hydration of the hexa-acylated Lipid A membrane (HPF2, **Table 2**).

In the present hPF-MD approach, the only difference between mono- (N^+) and divalent (N^{2+}) counterions in terms of CG parameters is the bead charge. Yet, the replacement of one N^{2+} by two N^+ particles led to a striking structural rearrangement of the bilayer, with the system of N^+ showing a persistent undulated configuration (**Figure 4**). This behavior is consistent with atomistic simulations

11

of Lipid-A bilayers, which have shown that Na^+ cations induce a significantly higher degree of disorder compared to Ca^{2+} (AA2, **Table 2**).[7] In particular, Pontes *et al.* speculated given the limited time and length scales reachable by atomistic models, that the non-lamellar arrangement of Lipid-A induced by replacement of Ca^{2+} by Na^+ is reminiscent of an inverted hexagonal H_{II} phase.[7] Indeed, LPS exhibits a rather complex structural polymorphism, with a strong dependence of the supramolecular aggregate structure on ambient conditions, and Lipid A has been shown to preferentially form non-lamellar structures under physiological conditions.[11,54,57]
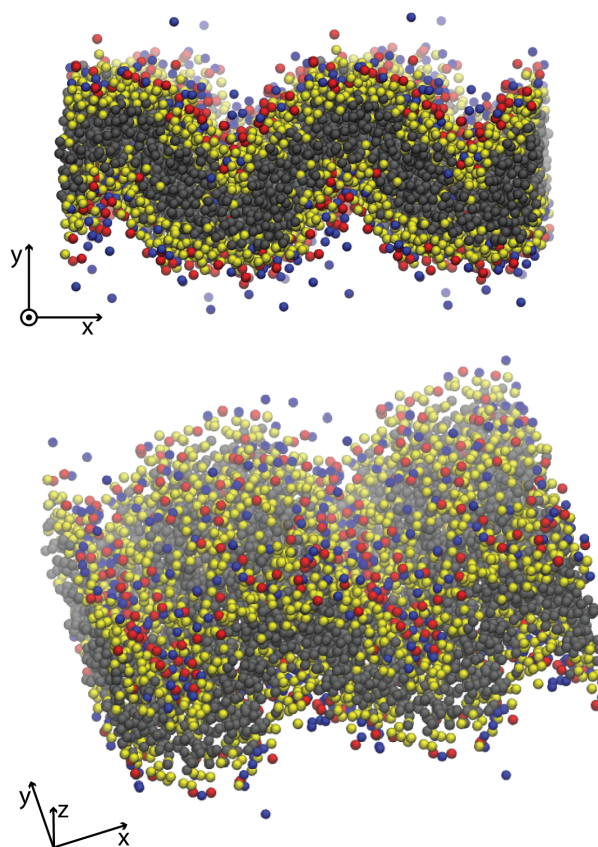
Figure 4. Structure of hexa-acylated Lipid A bilayer in the presence N^+ counterions. Color code: N^+ (blue), G/L (yellow), P (red) and C (gray). Water CG beads are not explicitly reported for clarity.

Transferability of χ parameters: hPF-MD simulations of tetra-acylated Lipid A. The length and the number of hydrophobic chains of Lipid A varies along different species (*e.g. Escherichia coli*, *Pseudomonas aeruginosa*, *Salmonella minnesota*). In order to assess whether CG intermolecular

interaction parameters obtained for hexa-acylated Lipid A (Table 1) are transferable to tetra-acylated lipids, we performed hPF-MD simulations for the latter system using N^{2+} counterions and a dielectric constant of $\epsilon_r = 15$ (HPF3, **Table 2**).
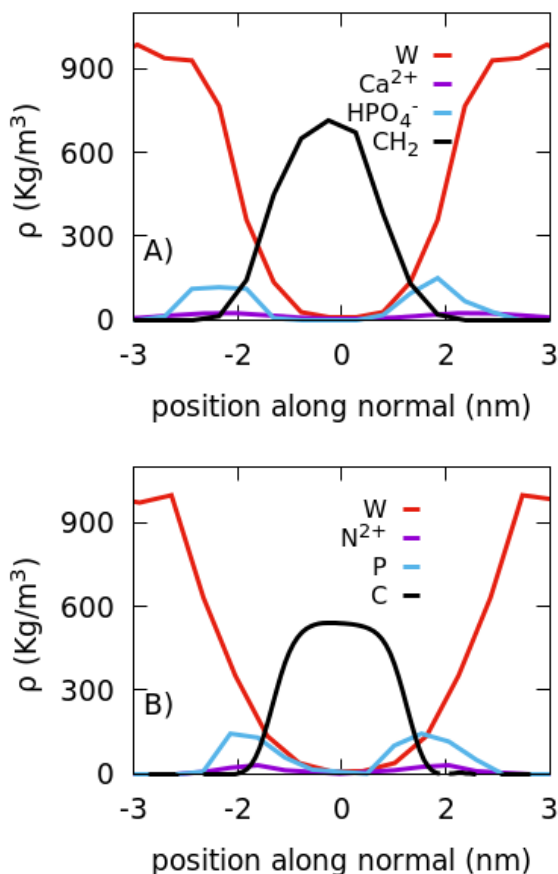

Figure 5. Mass density profile calculated along the normal direction of the tetra-acylated Lipid-A membrane plane for: A) reference tetra-acylated Lipid-A bilayer, B) hPF-MD simulation with $\epsilon_r = 15$. The profiles from hPF-MD simulation were calculated by averaging over the last 50 ns of the trajectory. The PO_4^{2-} curve corresponds to P beads (purple), CH_2 corresponds to C beads (yellow) and Ca_2^+ corresponds to N beads (blue). The water (W) curve is shown in red.

Comparison of density profiles calculated from all-atom (AA3, **Table 2**) and hPF-MD simulation results show that the corresponding peak positions of the hPF-MD curves are consistent with those in the reference atomistic simulation (**Figure 5**), apart from being less pronounced than those of the reference all-atom model, which is typical for such a CG modeling approach. This supports the transferability of the χ parameters between different Lipid A structures (e.g. number, length and position of acyl chains).

Self-Assembly of the Lamellar Phase. The present results indicate that the proposed model accurately reproduces the all-atom structural properties of pre-equilibrated Lipid A bilayers. To further validate our model, we verified its ability to describe self-assembly of the hexa-acylated Lipid A/N^{2+} mixtures in water. We studied two different concentrations (70 and 30 %$_{w/w}$ of water content, HPF4 and HPF5, **Table 2**) that, according to the experimental phase diagram, would produce significantly different stable assemblies. In particular, at lower concentration (70 % water), Lipid A should aggregate into a lamellar/cubic phase (L+Q), while at higher concentration (30 % water) it would produce a lamellar/hexagonal (L+H) state.

The stages along the self-assembly pathways, starting from random mixtures of Lipid A/water, are reported in **Figure 6**. For the system with 70% w/w of water, there is an initial stage of chaotic aggregation, which is followed by the formation of a bilayer structure around 1 µs, and finally a stable configuration is reached after 2.8 µs (**Figure 6A**). The equilibrium assembly structure is a coexistence of two phases, *i.e.* a planar bilayer (lamellar phase) which is fused with a cylindrical micelle (cubic phase), in agreement with the experimental phase diagram.[11,52] The system with lower water content (30 % w/w) reaches equilibrium after 1 µs. In this case, the self-assembled structure shows interconnected lamellae which are organised into an irregular honey-comb-like pattern (**Figure 6B**). This finding is also consistent with the experimentally observed (L+Q) aggregation.

The ability of hPF-MD to describe very different aggregation states for a single parameter set indicates that the model possesses adequatetransferability. In particular, the proposed model is able to describe surfaces with different coexisting curvatures, as highlighted in **Figure 6C,** where two sections (lateral and perpendicular) of the equilibrium conformation of the system with 70 % of water are reported.
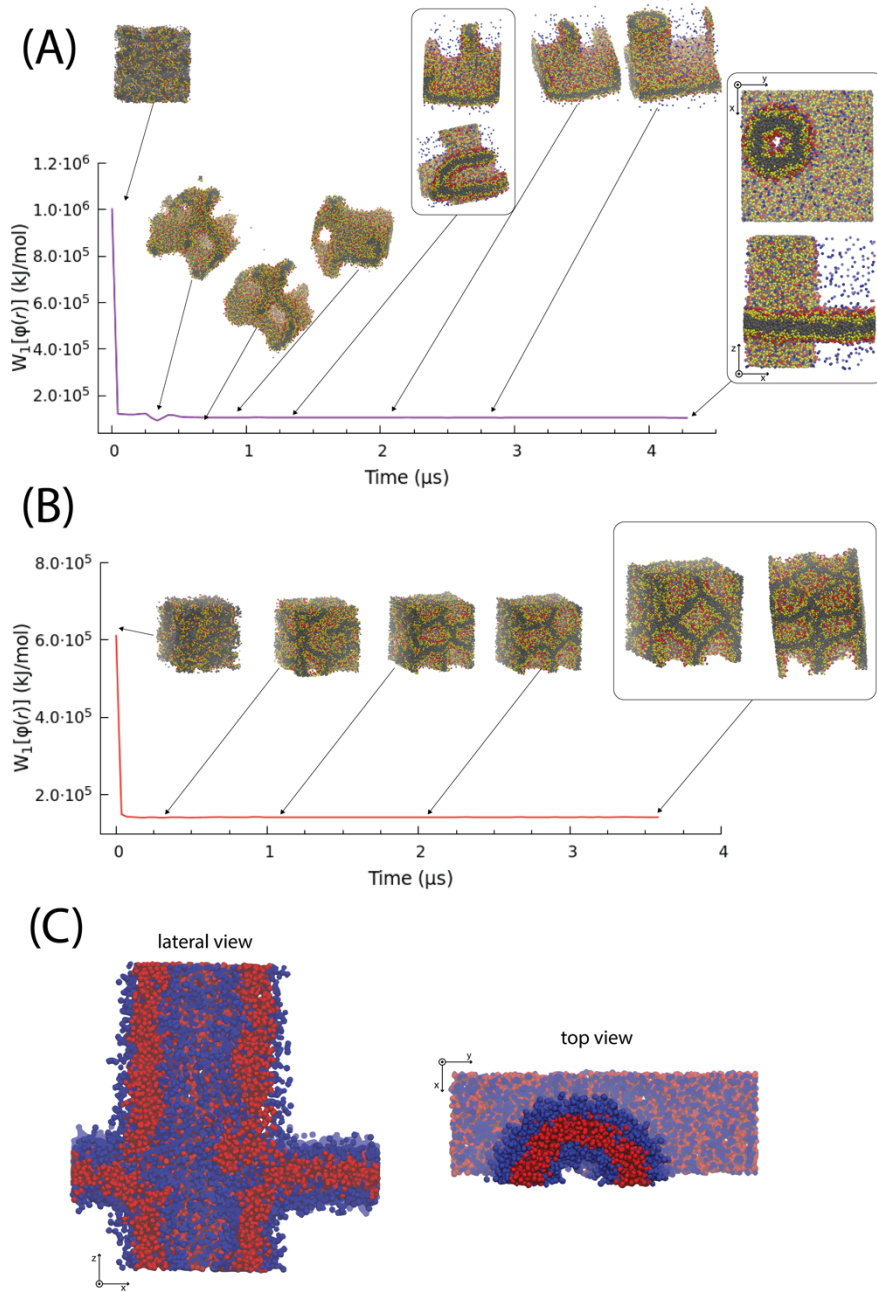
Figure 6. Time evolution of the $W_1[\{\phi(r)\}]$ potential for hexa-acylated Lipid A/water mixture (where $W_1[\{\phi(r)\}] = \frac{1}{2\phi_0}\int dr\, k_B T \sum_{K'} \chi_{KK'}\, \phi_K(r)\phi_{K'}(r)$ is the first term of the eq. 2): (A) 70% w/w of water, (B) 30% w/w of water. Representative snapshots are shown as insets. The color code used in the reported snapshots is the same as used in Figure 4. Water beads are not shown for clarity. Both simulations have been performed at 313 K. C) Lateral and top view of the equilibrium assembly for the 70% w/w system. To enhance the contrast, Lipid A head beads are shown in blue, while hydrophobic tails are shown in red. Ions and water beads are not shown for clarity.

Lipid A Vesicle. As a final test for the aggregation-propensity of Lipid A within our model, we investigated the structure of non-periodic vesicles in water. The vesicle consisted of 204 hexa-

acylated Lipid A molecules in the inner layer and 440 in the outer layer, with a total diameter of 15 nm (HPF6, **Table 2**) and an equal number of N^{2+} counterions placed close to the P beads in both layers. The time evolution of the vesicle radius, interaction potentials and representative snapshots of the vesicle structure indicate that the vesicle was stable within the simulated time (**Figure 8**). After the initial relaxation during the first 10 ns of the simulation, the vesicle retained a spherical shape with a radius of ~7.7 nm (**Figure 8B)**. Deviations from ideal sphericity are attributed to the non-stoichiometric binding of counterions in the outer layer, which reflect the instantaneous, strong repulsion between the phosphorylated heads. As a consequence, the effective head area for the different molecules that constitute the vesicle instantaneously changes, which produces structural deformations within the assembly. These findings indicate that liposome-like aggregates of hexa-acetylated Lipid A are stable, opening up a way to investigate how Lipid A activates proteins involved in the immune response of hosts.
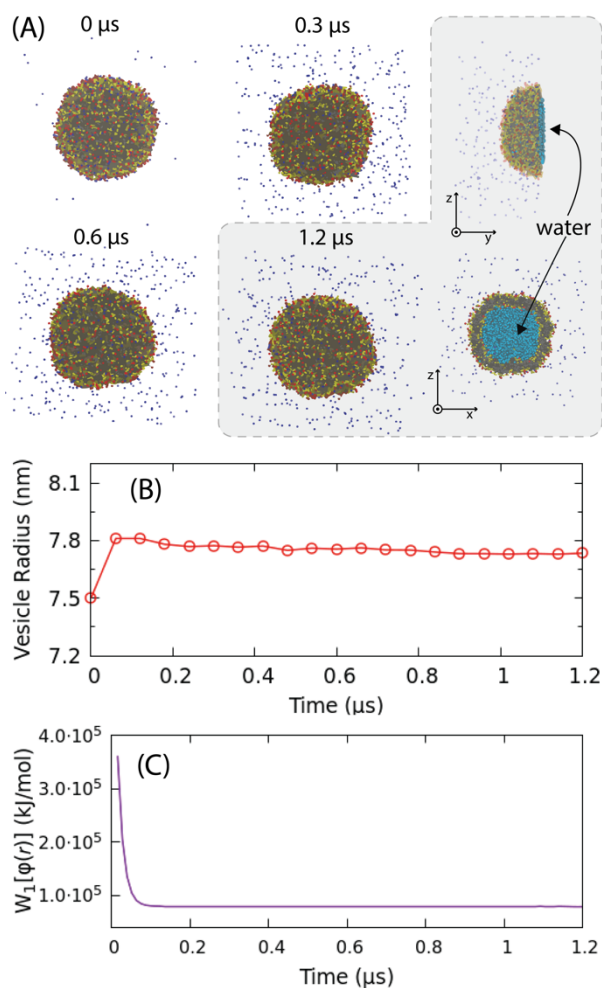
Figure 8. (A) Snapshots of Lipid A vesicle at different simulation times. For the last snapshot (at 1.2 μs) two sections of the vesicle with water inside its internal cavity are reported. For clarity, the water beads outside the vesicle are not shown. Bead types are reported using the same color code as in Figure 2. (B) Radius of the vesicle as a function of time. (C) Time evolution of the $W_1[\{\phi(r)\}]$ potential.

Conclusion

We presented a hPF-MD model for Lipid A that not only reproduces structural properties of atomistic simulations but also provides an experimentally-consistent description of the phase diagram of this complex glycolipid. The underlying molecular model employs a CG mapping similar to that of the Martini force-field, and most importantly, explicit electrostatic interactions to accurately represent mono and divalent counterions. The optimized set of parameters reproduce the lamellar phase of the reference all-atom models forconstituted Lipid A bilayers, with good qualitative and quantitative agreement of structural properties such as bilayer thickness, area per lipid, and density profiles.

The CG interaction parameters are transferable throughout chemical variants of Lipid A. Specifically, we verified the ability to reproduce the assembly characteristics for both hexa- and tetra-acylated Lipid A, as well as global structural modifications that are known to be induced by the presence of monovalent versus divalent counterions. Our model is also able to predict the self-assembly characteristics of Lipid A, and the spontaneous formation of complex L+Q or L+H phases as a function of the water/lipid concentration ratio. In particular, we observed the formation of complex structures that indicate coexistence of such phases, in agreement with the experimental phase diagram. The proposed model is able to describe interfaces of different curvature, ranging from infinite (planar bilayer) to finite curvature(inverted hexagonal and cubic assemblies). Finally, the stability of a Lipid A vesicle, starting from a pre-assembled configuration, has been investigated. We find that the vesicle is stable and remains spherical for over 1 µs of simulation time.

The optimized relative dielectric constant provides a proper description of the electrostatic interactions, which are of fundamental importance to correctly describe complex system such as Lipid A aggregates. These promising results encourage investigation of more complex lipopolysaccharide systems that are of key relevance for bio-medical studies.

References

[1]   H. Nikaido, Molecular Basis of Bacterial Outer Membrane Permeability Revisited, Microbiol. Mol. Biol. Rev. 67 (2003) 593–656. doi:10.1128/MMBR.67.4.593–656.2003.

[2]   S.G. Wilkinson, Bacterial lipopolysaccharides—Themes and variations, Prog. Lipid Res. 35

(1996) 283–343. doi:https://doi.org/10.1016/S0163-7827(96)00004-5.

[3]   N. Kućerka, E. Papp-Szabo, M.P. Nieh, T.A. Harroun, S.R. Schooling, J. Pencer, E.A. Nicholson, T.J. Beveridge, J. Katsaras, Effect of cations on the structure of bilayers formed by lipopolysaccharides isolated from Pseudomonas aeruginosa PAO1, J. Phys. Chem. B. 112 (2008) 8057–8062. doi:10.1021/jp8027963.

[4]   M. Caroff, D. Karibian, Structure of bacterial lipopolysaccharides, Carbohydr. Res. 338 (2003) 2431–2447. doi:https://doi.org/10.1016/j.carres.2003.07.010.

[5]   H. Ma, F.J. Irudayanathan, W. Jiang, S. Nangia, Simulating Gram-Negative Bacterial Outer Membrane: A Coarse Grain Model, J. Phys. Chem. B. 119 (2015) 14668–14682. doi:10.1021/acs.jpcb.5b07122.

[6]   A. Molinaro, O. Holst, F. Di Lorenzo, M. Callaghan, A. Nurisso, G. D'Errico, A. Zamyatina, F. Peri, R. Berisio, R. Jerala, J. Jiménez-Barbero, A. Silipo, S. Martín-Santamarí, Chemistry of lipid a: At the heart of innate immunity, Chem. - A Eur. J. 21 (2015) 500–519. doi:10.1002/chem.201403923.

[7]   F.J.S. Pontes, V.H. Rusu, T.A. Soares, R.D. Lins, The effect of temperature, cations, and number of Acyl chains on the lamellar to non-lamellar transition in Lipid-A membranes: A microscopic view, J. Chem. Theory Comput. 8 (2012) 3830–3838. doi:10.1021/ct300084v.

[8]   A.B. Schromm, K. Brandenburg, H. Loppnow, A.P. Moran, M.H.J. Koch, E.T.H. Rietschel, U. Seydel, Biological activities of lipopolysaccharides are determined by the shape of their lipid A portion, Eur. J. Biochem. 267 (2000) 2008–2013. doi:10.1046/j.1432-1327.2000.01204.x.

[9]   K. Brandenburg, U. Seydel, A.B. Schromm, H. Loppnow, M.H.J. Koch, E.T. Rietschel, Conformation of lipid A, the endotoxic center of bacterial lipopolysaccharide, Innate Immun. 3 (1996) 173–178. doi:10.1177/096805199600300302.

[10]   S.I. Miller, R.K. Ernst, M.W. Bader, LPS, TLR4 and infectious disease diversity, Nat. Rev.

Microbiol. 3 (2005) 36–46. doi:10.1038/nrmicro1068.

[11] K. Brandenburg, M.H.J.H.J. Koch, U. Seydel, Phase diagram of deep rough mutant lipopolysaccharide from Salmonella minnesota R595, J. Struct. Biol. 108 (1992) 93–106. doi:10.1016/1047-8477(92)90010-8.

[12] H. Reichelt, C.A. Faunce, H.H. Paradies, The phase diagram of charged colloidal lipid A-diphosphate dispersions, J. Phys. Chem. B. 112 (2008) 3290–3293. doi:10.1021/jp711720j.

[13] S. Khalid, T.J. Piggot, F. Samsudin, Atomistic and Coarse Grain Simulations of the Cell Envelope of Gram-Negative Bacteria: What Have We Learned?, Acc. Chem. Res. 52 (2019) 180–188. doi:10.1021/acs.accounts.8b00377.

[14] R.D. Lins, T.P. Straatsma, Computer simulation of the rough lipopolysaccharide membrane of Pseudomonas aeruginosa, Biophys. J. 81 (2001) 1037–1046. doi:10.1016/S0006-3495(01)75761-X.

[15] K.N. Kirschner, R.D. Lins, A. Maass, T.A. Soares, A glycam-based force field for simulations of lipopolysaccharide membranes: Parametrization and validation, J. Chem. Theory Comput. 8 (2012) 4719–4731. doi:10.1021/ct300534j.

[16] T.A. Soares, T.P. Straatsma, Assessment of the convergence of molecular dynamics simulations of lipopolysaccharide membranes, Mol. Simul. 34 (2008) 295–307. doi:10.1080/08927020701829880.

[17] A. Li, J.W. Schertzer, X. Yong, Molecular dynamics modeling of Pseudomonas aeruginosa outer membranes, Phys. Chem. Chem. Phys. 20 (2018) 23635–23648. doi:10.1039/c8cp04278k.

[18] E.L. Wu, O. Engström, S. Jo, D. Stuhlsatz, M.S. Yeom, J.B. Klauda, G. Widmalm, W. Im, Molecular dynamics and NMR spectroscopy studies of E. coli lipopolysaccharide structure and dynamics, Biophys. J. 105 (2013) 1444–1455. doi:10.1016/j.bpj.2013.08.002.

[19]   D.E.S.S. Santos, L. Pol-Fachin, R.D. Lins, T.A. Soares, Polymyxin Binding to the Bacterial Outer

Membrane Reveals Cation Displacement and Increasing Membrane Curvature in Susceptible

but Not in Resistant Lipopolysaccharide Chemotypes, J. Chem. Inf. Model. 57 (2017) 2181–

2193. doi:10.1021/acs.jcim.7b00271.

[20]   V.H. Rusu, R. Baron, R.D. Lins, PITOMBA: Parameter interface for oligosaccharide molecules

based on atoms, J. Chem. Theory Comput. 10 (2014) 5068–5080. doi:10.1021/ct500455u.

[21]   B. Van Oosten, T.A. Harroun, A MARTINI extension for Pseudomonas aeruginosa PAO1

lipopolysaccharide, J. Mol. Graph. Model. 63 (2016) 125–133.

doi:10.1016/j.jmgm.2015.12.002.

[22]   P.C. Hsu, B.M.H. Bruininks, D. Jefferies, P. Cesar Telles de Souza, J. Lee, D.S. Patel, S.J.

Marrink, Y. Qi, S. Khalid, W. Im, CHARMM-GUI Martini Maker for modeling and simulation

of complex bacterial membranes with lipopolysaccharides, J. Comput. Chem. 38 (2017).

doi:10.1002/jcc.24895.

[23]   F.A. Baltoumas, S.J. Hamodrakas, V.A. Iconomidou, The gram-negative outer membrane

modeler: Automated building of lipopolysaccharide-rich bacterial outer membranes in four

force fields, J. Comput. Chem. 40 (2019) 1727–1734. doi:10.1002/jcc.25823.

[24]   T Kawakatsu., Statistical physics of polymers: an introduction. Springer-Verlag, Berlin,

Heidelberg, 2004. ISBN 3-540-43440-2. pp 216, Polym. Int. (2005). doi:10.1002/pi.1772.

[25]   G. Milano, T. Kawakatsu, Hybrid particle-field molecular dynamics simulations for dense

polymer systems., J. Chem. Phys. 130 (2009) 214106. doi:10.1063/1.3142103.

[26]   T.A. Soares, S. Vanni, G. Milano, M. Cascella, Toward Chemically Resolved Computer

Simulations of Dynamics and Remodeling of Biological Membranes, J. Phys. Chem. Lett. 8

(2017) 3586–3594. doi:10.1021/acs.jpclett.7b00493.

[27]   S. J. Marrink, V. Corradi, P. C.T. Souza, H. I. Ingólfsson, D. Peter Tieleman, M. S.P. Sansom,

S.J. Marrink, P.C.T. Souza, V. Corradi, D.P. Tieleman, H.I. Ingólfsson, M.S.P. Sansom, Computational Modeling of Realistic Cell Membranes, Chem. Rev. 119 (2019) 6184–6226. doi:10.1021/acs.chemrev.8b00460.

[28] Y. Zhao, A. De Nicola, T. Kawakatsu, G. Milano, Hybrid particle-field molecular dynamics simulations: Parallelization and benchmarks, J. Comput. Chem. 33 (2012) 868–880. doi:10.1002/jcc.22883.

[29] A. De Nicola, Y. Zhao, T. Kawakatsu, D. Roccatano, G. Milano, Hybrid Particle-Field Coarse-Grained Models for Biological Phospholipids, J. Chem. Theory Comput. 7 (2011) 2947–2962. doi:10.1021/ct200132n.

[30] A. De Nicola, Y. Zhao, T. Kawakatsu, D. Roccatano, G. Milano, Validation of a hybrid MD-SCF coarse-grained model for DPPC in non-lamellar phases, Theor. Chem. Acc. 131 (2012) 1167. doi:10.1007/s00214-012-1167-1.

[31] E. Sarukhanyan, A. De Nicola, D. Roccatano, T. Kawakatsu, G. Milano, A. De Nicola, D. Roccatano, T. Kawakatsu, G. Milano, Spontaneous insertion of carbon nanotube bundles inside biomembranes: A hybrid particle-field coarse-grained molecular dynamics study, Chem. Phys. Lett. 595–596 (2014) 156–166. doi:10.1016/j.cplett.2014.01.057.

[32] A. De Nicola, T. Kawakatsu, G. Milano, A Hybrid Particle-Field Coarse-Grained Molecular Model for Pluronics Water Mixtures, Macromol. Chem. Phys. 214 (2013) 1940–1950. doi:10.1002/macp.201300214.

[33] A. De Nicola, S. Hezaveh, Y. Zhao, T. Kawakatsu, D. Roccatano, G. Milano, Micellar drug nanocarriers and biomembranes: how do they interact?, Phys. Chem. Chem. Phys. 16 (2014) 5093. doi:10.1039/c3cp54242d.

[34] A. De Nicola, T. Kawakatsu, C. Rosano, M. Celino, M. Rocco, G. Milano, Self-Assembly of Triton X-100 in Water Solutions: A Multiscale Simulation Study Linking Mesoscale to

Atomistic Models, J. Chem. Theory Comput. 11 (2015) 4959–4971.
doi:10.1021/acs.jctc.5b00485.

[35] A. Pizzirusso, A. De Nicola, G.J.A. Sevink, A. Correa, M. Cascella, T. Kawakatsu, M. Rocco, Y. Zhao, M. Celino, G. Milano, Biomembrane solubilization mechanism by Triton X-100: a computational study of the three stage model, Phys. Chem. Chem. Phys. 19 (2017) 29780–29794. doi:10.1039/C7CP03871B.

[36] S.L. Bore, G. Milano, M. Cascella, Hybrid Particle-Field Model for Conformational Dynamics of Peptide Chains, J. Chem. Theory Comput. 14 (2018) 1120–1130. doi:10.1021/acs.jctc.7b01160.

[37] Y.-L. Zhu, Z.-Y. Lu, G. Milano, A.-C. Shi, Z.-Y. Sun, Hybrid particle–field molecular dynamics simulation for polyelectrolyte systems, Phys. Chem. Chem. Phys. 18 (2016) 9799–9808. doi:10.1039/C5CP06856H.

[38] H.B. Kolli, A. De Nicola, S.L. Bore, K. Schäfer, G. Diezemann, J. Gauss, T. Kawakatsu, Z. Lu, Y.-L.Y. Zhu, G. Milano, M. Cascella, Hybrid Particle-Field Molecular Dynamics Simulations of Charged Amphiphiles in an Aqueous Environment, J. Chem. Theory Comput. 14 (2018) 4928–4937. doi:10.1021/acs.jctc.8b00466.

[39] S.L. Bore, H.B. Kolli, T. Kawakatsu, G. Milano, M. Cascella, Mesoscale Electrostatics Driving Particle Dynamics in Nonhomogeneous Dielectrics, J. Chem. Theory Comput. 15 (2019) 2033–2041. doi:10.1021/acs.jctc.8b01201.

[40] M. Alfaraj, Y. Wang, Y. Luo, Enhanced isotropic gradient operator, Geophys. Prospect. 62 (2014) 507–517. doi:10.1111/1365-2478.12106.

[41] G.J.A. Sevink, F. Schmid, T. Kawakatsu, G. Milano, Combining cell-based hydrodynamics with hybrid particle-field simulations: efficient and realistic simulation of structuring dynamics, Soft Matter. 13 (2017) 1594–1623. doi:10.1039/c6sm02252a.

[42]   Y. Zhao, A. De Nicola, T. Kawakatsu, G. Milano, Parallelization and benchmark, J. Comput. Chem. 33 (2012) 868–880.

[43]   S.J. Marrink, H.J. Risselada, S. Yefimov, D.P. Tieleman, A.H. De Vries, The MARTINI force field: Coarse grained model for biomolecular simulations, J. Phys. Chem. B. 111 (2007) 7812–7824. doi:10.1021/jp071097f.

[44]   G. Bussi, D. Donadio, M. Parrinello, Canonical sampling through velocity rescaling, J. Chem. Phys. 126 (2007) 14101. doi:10.1063/1.2408420.

[45]   H.J.C. Berendsen, J.P.M. Postma, W.F. van Gunsteren, A. DiNola, J.R. Haak, Molecular dynamics with coupling to an external bath, J. Chem. Phys. 81 (1984) 3684–3690. doi:10.1063/1.448118.

[46]   L. Martínez, R. Andrade, E.G. Birgin, J.M. Martínez, Software News and Update Packmol: A Package for Building Initial Configurations for Molecular Dynamics Simulations, J. Comput. Chem. 30 (2009) 2157–2164.

[47]   H.C. Andersen, Molecular dynamics simulations at constant pressure and/or temperature, J. Chem. Phys. 72 (1980) 2384–2393. doi:10.1063/1.439486.

[48]   L. Pol-Fachin, V.H. Rusu, H. Verli, R.D. Lins, GROMOS 53A6 GLYC, an improved GROMOS force field for hexopyranose-based carbohydrates, J. Chem. Theory Comput. (2012). doi:10.1021/ct300479h.

[49]   H. J. C. Berendsen, J. R. Grigera, T. P. Straatsma, The missing term in effective pair potentials, J. Phys. Chem. 91 (2002) 6269–6271. doi:10.1021/j100308a038.

[50]   B. Hess, H. Bekker, H.J.C. Berendsen, J.G.E.M. Fraaije, LINCS: A linear constraint solver for molecular simulations, J. Comput. Chem. 18 (1997) 1463–1472. doi:10.1002/(SICI)1096-987X(199709)18:12<1463::AID-JCC4>3.0.CO;2-H.

[51]   B. Hess, C. Kutzner, D. van der Spoel, E. Lindahl, GROMACS 4: Algorithms for Highly Efficient,

Load-Balanced, and Scalable Molecular Simulation, J. Chem. Theory Comput. 4 (2008) 435–447. doi:10.1021/ct700301q.

[52] K. Brandenburg, M.H.J. Koch, U. Seydel, Phase diagram of lipid A from Salmonella minnesota and Escherichia coli rough mutant lipopolysaccharide, J. Struct. Biol. 105 (1990) 11–21. doi:10.1016/1047-8477(90)90093-R.

[53] S. Snyder, D. Kim, T. J. McIntosh, T.J. McIntosh, Lipopolysaccharide Bilayer Structure: Effect of Chemotype, Core Mutations, Divalent Cations, and Temperature, Biochemistry. 38 (1999) 10758–10767. doi:10.1021/bi990867d.

[54] P. Garidel, M. Rappolt, A.B. Schromm, J. Howe, K. Lohner, J. Andrä, M.H.J. Koch, K. Brandenburg, Divalent cations affect chain mobility and aggregate structure of lipopolysaccharide from Salmonella minnesota reflected in a decrease of its biological activity, Biochim. Biophys. Acta - Biomembr. 1715 (2005) 122–131. doi:10.1016/j.bbamem.2005.07.013.

[55] C. Jeworrek, F. Evers, J. Howe, K. Brandenburg, M. Tolan, R. Winter, Effects of specific versus nonspecific ionic interactions on the structure and lateral organization of lipopolysaccharides, Biophys. J. 100 (2011) 2169–2177. doi:10.1016/j.bpj.2011.03.019.

[56] A. Nascimento, F.J.S. Pontes, R.D. Lins, T.A. Soares, Hydration, ionic valence and cross-linking propensities of cations determine the stability of lipopolysaccharide (LPS) membranes, Chem. Commun. 50 (2014) 231–233. doi:10.1039/c3cc46918b.

[57] K. Brandenburg, W. Richter, M.H.. Koch, H.. Meyer, U. Seydel, Characterization of the nonlamellar cubic and HII structures of lipid A from Salmonella enterica serovar Minnesota by X-ray diffraction and freeze-fracture electron microscopy, Chem. Phys. Lipids. 91 (1998) 53–69. doi:10.1016/S0009-3084(97)00093-5.